Available online at www.sciencedirect.com
SCIENCE DIRECT®
Cement & Concrete Composites 27 (2005) 934–944
Cement & Concrete Composites
www.elsevier.com/locate/cemconcomp

Reinforced polymer concrete: Physical properties of the matrix and static/dynamic bond behaviour

J. Tomás San-José [a,b,*], Iñigo Vegas [a], Antonio Ferreira [c]

[a] LABEIN. c/Geldo, Parque Tecnológico de Bizkaia, Edificio 700, 48160-Derio (Vizcaya), Spain
[b] UPV-EHU Basque Country University, ESI de Bilbao, Alda. Urquijo s/n. 48013 Bilbao, Spain
[c] FEUP Faculdade de Engenharia da Universidade do Porto, Rua Dr. Roberto Frias, 4200-465 Porto, Portugal

Received 27 November 2003; accepted 7 June 2005
Available online 15 August 2005

Abstract

The paper aims at analysing the performance of Polyester Polymer Concrete (PPC) reinforced with steel and FRP rebars. The PPC is also compared with conventional cement concrete.

On the one hand, the effect of the polymer matrix microstructure on the mechanical performance (compression and flexural strength, deformability and Young's modulus) is discussed.

On the other hand, static and dynamic bond behaviour under pure pull-out forces between the PPC and different rebars is tackled. It is analysed the behaviour of metallic and non-metallic rebars embedded in a PPC matrix when they are subjected to both monotonic and cyclic loads. Likewise, analogous tests were performed on cement concrete specimens in order to be able to compare the bonding performance in both types of concrete.

1. Introduction

The polyester polymer concrete (PPC) studied in the present paper is a construction material comprising three phases: inorganic (aggregates), organic (thermosetting polyester resin) and inert (air porosity due to fabrication process). Most of current applications for PPC in Europe relate to precast building elements and some structural components in civil works such as slabs and façade panels.

Two different PPCs, based on orthophthalic and isophthalic resins, are analysed in this work. Each PPC corresponds to different processes, raw materials and applications. Therefore, it will be difficult to draw general conclusions. Likewise, the present study is constantly subjected to uncertainties due to the design, manufacturing and transportation of the specimens.

This research is part of the European Project Plasticrete [1] investigating the development of new reinforced materials in construction. The work presented in this paper was undertaken at LABEIN facilities in Bilbao (Spain).

2. Material specifications

The dosage of the polyester polymer concretes, used in the present work, is presented in both Tables 1 and 2. Both type U and type G are made of two different thermosetting polyester resins; namely, isophthalic and orthophthalic. The PPC type U (isophthalic polyester polymer concrete) and G (orthophthalic polyester polymer concrete) come from different industrial plants. The casting process has therefore produced two different materials, not only from a chemical composition point

* Corresponding author. Address: LABEIN. c/Geldo, Parque Tecnológico de Bizkaia, Edificio 700, 48160-Derio (Vizcaya), Spain.
E-mail address: labein@labein.es (J.T. San-José).

0958-9465/$ - see front matter © 2005 Elsevier Ltd. All rights reserved.
doi:10.1016/j.cemconcomp.2005.06.004

Table 1
Isophthalic polyester PPC components dosage

Component	PPC type U (%)
Polyester resin type and content	12
Catalyst peroxide	2[a]
Accelerator (cobalt octoate)	6[a]
TiO_2 colour additive	2.5
Carbonate filler (0.05–0.2 mm)	21.4
Quartz fine sand (0.2–0.5 mm)	49.6
Quartz sand (0.5–5 mm)	14.5

[a] With regard to the resin content.

Table 2
Ortophthalic polyester PPC components dosage

Component	PPC type G (%)
Resin-mix	12.3
Quartz fine sand	24.7
Quartz gravel	49.3
Quartz powder	6.7
Chalk	7

of view, but also from the microstructural one. In this sense, it is a key aspect to analyse the role of the microscopic distribution of the components (resin, aggregates and air) in the fundamental mechanical performance [2–4].

3. Macroscopic study

From a mechanical (macroscopic) point of view, there are several fundamental properties to have in mind; namely, the compressive stress–strain curve, the flexural strength and the static elastic modulus.

3.1. Compressive stress–strain curves

The compressive stress–strain curves as well as the calculation of static elastic modulus and Poisson's ratio values were conducted based on the RILEM method TC 113-CPT (PC-8) [5]. Cylindrical specimens (∅ 100 mm × 200 mm) were used in these tests. For measuring the static longitudinal and transversal strain of the specimens, wires of the strain measuring apparatus were attached to two diametrically opposite gages, which were positioned parallel to the axis and centred about mid-height of the specimen. During the test, the longitudinal strains as the compressive strains were measured at appropriate load intervals, in such a way as in San-Jos¯'s [6]. The transversal strains were used for calculating the Poisson's ratio. Both the modulus of elasticity and Poisson's ratio are applicable within the customary elastic working stress range (0–40% of ultimate concrete strength). The static elastic modulus of the concrete was calculated through the following equation:

$$\boldsymbol{E} = (S_1 - S_2)/(\varepsilon - 0.000050)$$

where $\boldsymbol{E}$ is the static elastic modulus as chord modulus (MPa), S_1 is the compressive stress corresponding to a compressive strain of 50 millionths (MPa); S_2 is the compressive stress corresponding to a 40%. of maximum load (MPa), ε is the longitudinal strain produced by a compressive stress S_2 (millionths). The Poisson's ratio of the concrete was calculated through the following equation:

$$\boldsymbol{\mu} = (\varepsilon_{t2} - \varepsilon_{t1})/(\varepsilon - 0.000050)$$

where $\boldsymbol{\mu}$ is the Poisson's ratio, $\varepsilon_{t2}$is the transverse strain at midheight of specimen produced by stress S_2, ε_{t1} is the transverse strain at midheight of specimen produced by stress, $S_1\varepsilon$ is the longitudinal strain produced by a compressive stress S_2.

Both types of polymer concrete were analysed to obtain the fundamental stress–strain parameters in compression (Table 3). The most effective comparative analysis of these type U and G, in compression, can be observed in their respectively stress vs strain curves. Fig. 1 shows the mentioned average curves corresponding to diverse test specimens. Important mechanical behaviour differences under compression loads can be noted when comparing the two types of polymer concrete tackled in the present work. All of them will

Table 3
PPC types U and G compression parameters

Properties	Type U	Type G
Strength (MPa)	92.0	102
Young modulus (MPa)	24,863	30,492
Poisson ratio	0.23	0.21
Maximum strain (‰)	6.5	5.0

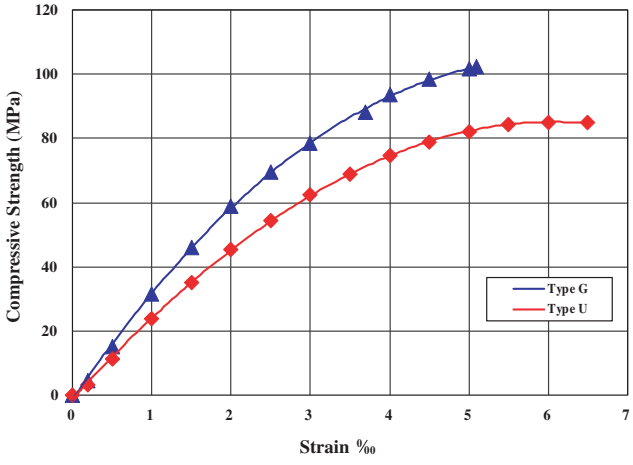

Fig. 1. Compression stress vs strain PC.

be discussed from the microstructural point of view by using different experimental techniques.

3.2. Flexural behaviour

The flexural strength was conducted based on the RILEM method TC 113-CPT (PC-7) [5]. Prismatic specimens ($40 \times 40 \times 160$ mm) were used in these tests. For measuring the deformation of the specimens, gauges were positioned at mid-span, centred at mid-height of the specimens, based on the work developed in [6].

Fig. 2 shows the curves corresponding to average values from various specimens subjected to bending loads. As mentioned above, PPC type U and G (12% resin content) were analysed in order to obtain the fundamental stress vs strain parameters in bending (Table 4).

4. Microscopic study

The microstructural analysis was articulated into the following techniques: intrusion porosimetry and scanning electron microscopy (SEM). The first technique was used for studying the internal porosity distribution, while the second one was used for determining the aspect of the interface between the resin and the aggregates.

4.1. Internal pore distribution

The intrusion porosimetry is a commonly extended analysis technique in the petrography and concrete durability field. It deals basically with analysing the penetration of a liquid in the porosity of the specimen material to be studied, via the intrusion at low (0.34 MPa) and high (414 MPa) pressure of the mercury. Pore volume is calculated by determining the volume of mercury

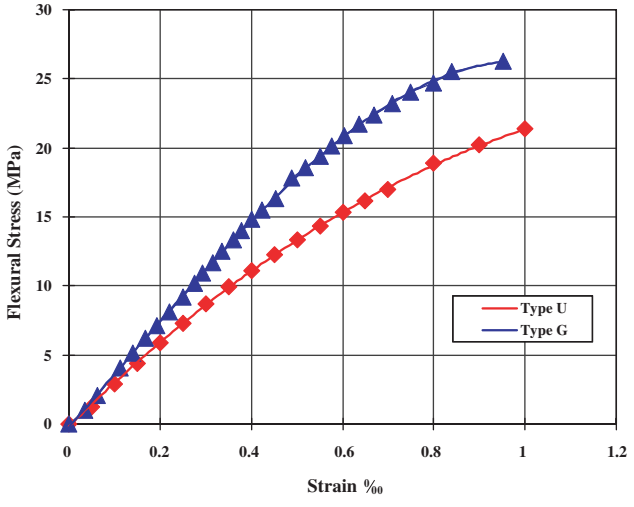

Fig. 2. Flexural stress vs strain in PPC.

Table 4
PPC types U and G flexural parameters

Properties	Type U	Type G
Strength (MPa)	21.5	26.0
Young modulus (MPa)	28,710	37,868
Maximum strain (‰)	1.0	0.98

remaining in the penetrometer stem. As pressure increases, mercury moves into the sample pores, vacating the stem. Intrusion of different size pores occurs at different pressures.

The greater pressure, the smallest is the pore diameter into which the mercury can be forced. As the mercury shows a high surface tension and is non-wetting to most materials, its angle of contact and radius of curvature can be used to calculate the pore diameter into which it is intruded at a given pressure. Therefore, it is possible to obtain the total porosity and bulk, as well as the apparent density (see Table 5).

The porosimetry study reveals the following key aspects:

- The type U shows larger number of pores than the type G.
- The porosity and the maximum pore size are higher in the type U than in the type G.
- Both concretes are formed of internal closed pores.

The internal pore distribution and pore aspect of the analysed polymer concretes can be observed in Figs. 3 and 4. This technique was undertaken to observe the interface between aggregates and resin. As referenced in San-José et al. [7], this area configuration is one of the most important aspects to understand the macroscopic performance in both types of concrete. The sample preparation was performed by covering them with a gold layer under vacuum conditions of 3×10^{-2} mbar during a covering time of 1 min 50 s with 15 mA of sputtering.

4.2. Scanning electron microscopy (SEM)

As shown in the Fig. 5, the resin matrix of the type U concrete creates a thinner layer of resin surrounding the aggregate, than the type G (Fig. 6).

On the other hand, the irregular shapes of the aggregates in the type G concrete, together with the higher

Table 5
PPC types U and G porosimetry intrusion

PPC type	Porosity (%)	Density (kg/m^3)	
		Apparent	Bulk
U	7.3	2150	2320
G	4.8	2270	2390

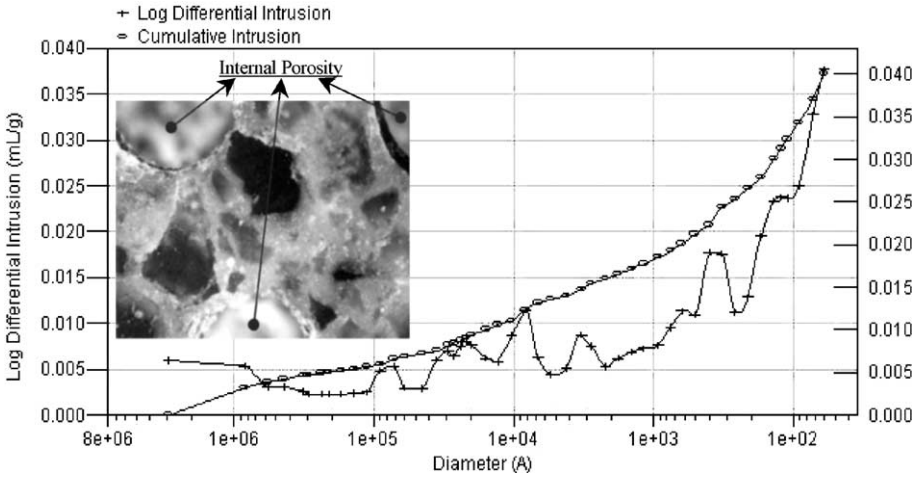

Fig. 3. Porosimetry intrusion and aspect. PPC type U.

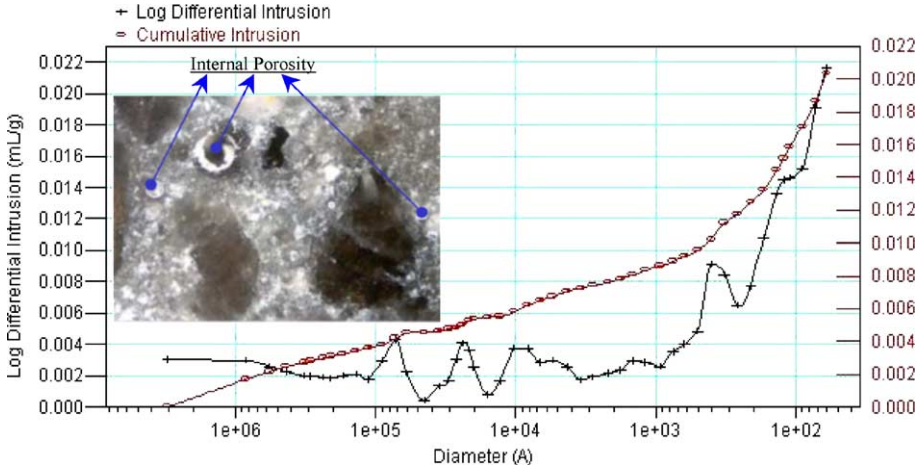

Fig. 4. Porosimetry intrusion and aspect. PC type G.

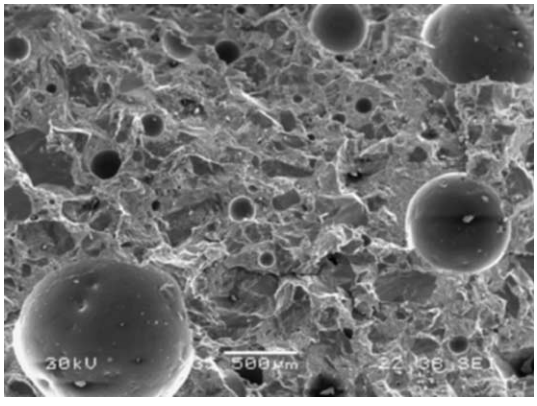

Fig. 5. SEM microphotograph of PPC-U (×35).

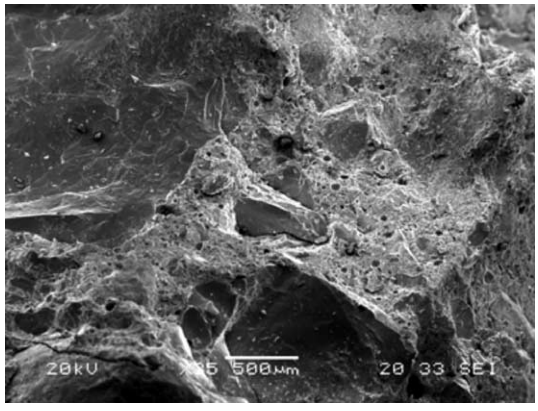

Fig. 6. SEM microphotograph of PPC-G (×35).

size, improve the anchorage with the resin matrix. Therefore, it can be said that the type G concrete is, from a microscopic point of view, a more compacted material than the type U one. Furthermore, a big difference in size of the air voids was observed in both PPCs. This aspect is basically due to the manufacturing process to aspects such as mixer design, moulding and post-curing conditions.

Likewise, the specific area of the aggregates to be wet (same resin content), increase the internal differences showed in the previous two figures analysed by SEM. On the other hand, the fact of using two different resin formulations and aggregates does not influence so much the microscopic aspect as the casting process.

5. Relationship between macro- and micro-parameters

The fundamental results of the macro- and micro-study, for the type U and G polymer concretes, are respectively summarized in Table 6. From the results, it can be concluded that porosity, aggregates-matrix interface, strength and deformability are narrowly linked.

The type U reveals 6040 m^2/g of average pore area, while type G concrete shows 3484 m^2/g. Based on the latter results, the discontinuity effect due to the size and pore distribution can also be explained. Moreover, the type G concrete shows a more compacted interface (the resin layer enveloping the aggregates is wider) than the type U. In other words, the structure of the type G concrete presents 42% higher continuity to transfer the loads, and consequently, it shows an improved mechanical behaviour and lower deformations than type U.

The casting process is the most important aspect in which the different behaviour of the studied polyester polymer concretes lays. The analysed polymer concretes have the same resin content. Therefore, the matrix formulations seem not to be so different as for being a key factor in the micro–macroscopic relationship. The aggregate shape and size might be another reason to justify the different micro- and macro-behaviour of the studied polymer concretes.

On the basis of the above discussions, it can be easily understood why the type U concrete is used for façade elements and the type G one is used for producing structural elements such as reinforced slabs.

6. Polyester polymer concrete in bonding

The bond mechanism of rebars to concrete is the phenomenon on which is based the structural behaviour of this composite. The following sections present the bond study of different reinforced PPC subjected to both monotonic and cyclic loading. The tests described in the following sections deal with steel and GFRP (Glass Fibre Reinforced Plastic) bars, ACI [8], embedded in cement and polymer concrete and subjected to monotonic and cyclic tensile load.

6.1. Monotonic bond test

Three types of concrete were used for casting the specimens; namely, ordinary cement concrete (CC), CPH [9], used as reference for comparison with the polymer composite, isophthalic polyester polymer concrete (type U PPC), and orthophthalic polyester polymer concrete (type G PPC). Polymer concretes were elaborated with 12% of resin content. Table 7 shows the mechanical properties of the concretes used for developing the bonding study. As can be observed, values in Table 7 are of similar magnitude to those given in Tables 3 and 4 corresponding to previous mixes for the material characterisation. There is a slight variation among values in the mentioned tables because of the scatter of test results in concrete.

On the other hand, three types of rebars were used during this research. Steel as metallic reinforcement and GFRP as non-ferrous reinforcement. Within the GFRP rods, square sand-coated profiles and round smooth bars were considered. Table 8 shows the mechanical properties of the reinforcement used for developing this study.

The specimen adopted for this test consisted of a 500 mm long bar embedded partially in a concrete cube ($150 \times 150 \times 150$ mm). The embedment length was

Table 6
PPCs types U and G summary micro- and macro-results

PPC	Macroscopic properties			Microscopic properties	
	Compression		Bending strength (MPa)	Pores content (%)	Bulk density (kg/m^3)
	Strength (MPa)	Strain (‰)			
U	92	6.5	21.5	7.3	2320
G	102	5.0	26	4.8	2390

Table 7
Properties for PPC and CC

Property (MPa)	Type of concrete		
	CC	PPC type U	PPC type G
Compressive strength	48.5	85.9	96.5
Longitudinal modulus	36,361.5	24,863	30,492
Flexural strength	6.2	18.8	26

Note: The values presented in this table correspond to specific batches performed for the bond study.

Table 8
Properties for metallic and non-ferrous rebars

Property	Bar type		
	Steel	GFRP square	GFRP round smooth
Tensile strength (MPa)	550	1100	1000
Tensile modulus (GPa)	200	45	45
Failure strain (%)	22	2.5	2.5

designed in multiples of the bar diameter or side of the bar. The two ends of the bar in the concrete cube were isolated, using plastic bushes or several layers of cling film, in order to avoid the adherence in those parts of the specimen. The diameter or side of the rods was 8 mm. The adherence length in the polymer concrete specimens was 24 mm while in the cement concrete was 48 mm, in accordance with the criteria shown in Table 9. Previous investigations had already shown that the bond capacity of rebars in cement concrete was considerably lower than in polymer concrete. Based on it, and in order to assure the sensitivity in the pull-out test, it was considered twice bond length in cement concrete with regard to that established for polymer concrete. Bond tests were conducted taking into consideration the works of Fowler [4]. The specimen was vertically positioned in a RIEHLE loading apparatus as illustrated in Fig. 7. The load on the reinforcing bar was applied at a loading rate not greater than 22 kN/min. A dial gauge was used for measuring the slip of the bar at the free-unloaded end of the bar. At slips of 0.01 mm, 0.1 mm and 1 mm, the respective loads were recorded. The bond stress for every measurement was calculated in accordance with the Eq. (1) for round sections and (2) for square sections:

$$\tau_i = \frac{F_i}{L \cdot \pi \cdot \phi}, \tag{1}$$

$$\tau_i = \frac{F_i}{L \cdot 4 \cdot l}, \tag{2}$$

where τ_i = bond stress (MPa) corresponding to "i" mm slip; F_i = load (N) corresponding to "i" mm slip; ϕ = diameter of the round bar (mm); l = side of the square profile (mm); L = embedment length (mm). The mean bond stress, according to the recommendations of CPH [9], was determined using the relationship (3):

$$\tau_b = \frac{\tau_{0.01} + \tau_{0.1} + \tau_1}{3} \tag{3}$$

It must be highlighted that for those specimens where the bond failure occurred at slips lower than 1 mm, the equation above was not directly applied. In such cases, the bond strength was obtained as an arithmetic mean of the recorded values before bond failure occurred. In GFRP smooth rebars, for example, the bond failure occurred at slips lower than 0.1 mm, calculating the bond strength from an unique value corresponding to the recorded value in failure.

This mode of calculation provides a safer value of the bond strength than that considering the maximum pull-out load. Test results are shown in Tables 10–12. The failure modes during the pull-out test are also indicated in the tables. Table 13 presents the mean values of bond strength for the different rebars to concrete.

This study presents a conservative mode of calculating the bond strength, since this has been determined as a mean value of three stress levels corresponding to different slips. The purpose of this work was to establish a comparative study of the bond resistance for various reinforced concretes. However, if it was required to adjust the capacity of anchorage of a structural element, an approach based on the maximum pull-out load should be undertaken.

From the results of pull-out tests carried out on the dealt concretes, the following conclusions can be drawn:

- The sand-coated GFRP reinforced polyester polymer concrete (PPC) provides values of the bonding strength similar to traditional steel reinforced concretes.
- In PPC, steel bars allow bonding strengths 70% greater than GFRP rods.

Table 9
Adherence length depending on concrete and rebar type

Concrete type	Adherence length			
	Steel	GFRP square		GFRP round smooth
		Type 1	Type 2	
PPC	$3 \cdot \phi$	$3 \cdot 1$	$3 \cdot 1$	$3 \cdot \phi$
CC	$6 \cdot \phi$	$6 \cdot 1$	$6 \cdot 1$	$6 \cdot \phi$

Type 1 and type 2 bars are sand coated, ϕ is the diameter of the round bars, l is the side of the square bars.

Fig. 7. Pull-out set up.

Table 10
PPC type G detailed pull-out results

Bar type	Specimen	Bond stress at different slips (MPa)			Average (MPa)		Failure mode
		0.01 mm	0.1 mm	1 mm			
Steel	G01	12.2	20.5	38.7	23.8	24.4	Bond
	G02	14.9	22.2	37.5	24.9		
	G03	9.6	17.8	32.0	19.8		
	G04	17.1	24.1	42.3	27.8		
	G05	13.7	23.6	39.1	25.5		
GFRP type 1	GI1	5.8	17.6	–	11.7	14.0	Slip at 0.38 mm
	GI2	9.0	15.9	19.0	14.7		Bond
	GI3	7.8	14.6	19.8	14.1		
	GI4	10.4	16.2	19.6	15.4		
GFRP type 2	GII1	5.4	15.1	19.9	13.5	13.9	Bond
	GII2	9.1	18.3	22.0	16.5		
	GII3	8.1	13.4	17.2	12.9		
	GII4	7.4	16	20.1	14.5		
	GII5	7.3	17.3	–	12.3		Slip at 0.35 mm
GFRP smooth	GIII1	Crack of the bar				14.9	Splitting
	GIII2	7.8	–	–	7.8		Slip at 0.05 mm
	GIII3	20.2	–	–	20.2		Slip at 0.08 mm
	GIII4	19.1	–	–	19.1		Slip at 0.01 mm
	GIII5	12.3	–	–	12.3		Slip at 0.02 mm

Table 11
PPC type U detailed pull-out results

Bar type	Specimen	Bond stress at different slips (MPa)			Average (MPa)		Failure mode
		0.01 mm	0.1 mm	1 mm			
Steel	U01	14.0	27.5	50.9	30.8	30.4	Bond
	U02	18.5	32.4	–	25.5		Bond tension failure
	U03	20.7	39.2	–	29.9		
	U04	22.3	39.1	–	30.7		
	U05	14.9	32.1	57.9	35.0		Bond
GFRP type 1	UI1	11.4	22.6	–	17.0	18.0	Slip at 0.46 mm
	UI2	11.6	23.9	–	17.8		Slip at 0.33 mm
	UI3	12.4	19.0	22.8	18.1		Bond
	UI4	13.6	24.3	–	19.0		Slip at 0.46 mm
	UI5	11.9	24.5	–	18.2		Slip at 0.4 mm
GFRP type 2	UII1	9.5	23.7	–	16.6	19.0	Slip at 0.32 mm
	UII2	11.8	24.3	–	18.0		Slip at 0.35 mm
	UII3	12.6	23.8	28.4	21.6		Bond
	UII4	14.3	24.9	–	19.6		Slip at 0.29 mm
	UII5	12.7	26.1	–	19.4		Slip at 0.36 mm
GFRP smooth	UIII1-2	2.0	2.6	4.1	2.9	3.6	Bond
	UIII2-2	2.5	2.7	3.8	3.0		
	UIII3-2	2.0	3.3	5.9	3.8		
	UIII4-2	2.6	3.9	6.2	4.2		
	UIII5-2	2.5	3.9	6.5	4.3		

- In cement concrete, steel bars allow bonding strengths 25% greater than GFRP rods.
- Smooth non-metallic rebars, though considerable cheaper than textured ones, do not generate sufficient bond strength and should be avoided.
- The square bar profile provides a greater bond surface area/volume ratio.

6.2. Dynamic bond test

This section aims at studying the bond mechanism of GFRP rebars to polymer concrete when subjected to cyclic loading. Four types of specimens were tested in order to compare new possibilities with traditional ones. Two types of concretes were used for manufacturing the

Table 12
CC (ordinary concrete) detailed pull-out results

Bar type	Specimen	Bond stress at different slips (MPa)			Average (MPa)		Failure mode
		0.01 mm	0.1 mm	1 mm			
Steel	I01	6.5	10.9	16.4	11.3	12.5	Bond
	I02	6.3	12.1	18.0	12.1		
	I03	6.9	12.3	17.5	12.2		
	I04	9.7	13.9	17.2	13.6		
	I05	8.2	13.4	17.6	13.1		
GFRP type 1	I-I1	6.7	10.2	7.5	8.1	9.7	
	I-I2	10.3	12.9	9.5	10.9		
	I-I3	6.7	9.4	7.3	7.8		
	I-I4	10.4	13.0	10.7	11.4		
	I-I5	9.2	12.1	9.2	10.2		
GFRP type 2	I-II1	8.6	11.9	9.8	10.1	9.9	
	I-II2	9.1	10.9	8.0	9.3		
	I-II3	10.1	12.2	9.3	10.5		
	I-II4	8.7	11.7	9.3	9.9		
	I-II5	8.4	11.7	9.2	9.8		
GFRP smooth	I-III1		Fast slip		1.0	0.8	
	I-III2	0.9	1.0	0.6	0.8		
	I-III3	1.0	1.1	0.6	0.9		
	I-III4	0.5	0.5	0.3	0.4		
	I-III5		Fast slip		0.9		

Table 13
Bond strength between different concretes and rebars combinations

Type of concrete	Bond strength (MPa)			
	Steel	GFRP square		GFRP round smooth
		Type 1	Type 2	
PPC type G	24.4	14.0	13.9	14.9
PPC type U	30.4	18.0	19.0	3.6
CC	12.5	9.7	9.9	0.8

samples; namely, ordinary cement concrete (CC) and orthophthalic, 12% resin content, polyester polymer concrete (PPC type G of past sections). See Table 7 for properties. Two types of rebars were used. Steel as metallic rebar and GFRP square sand-coated profiles as non-metallic rebars. See Table 8 for properties. Like the samples cast for the monotonic pull-out tests, the specimens used for bonding fatigue were formed of cubic blocks ($150 \times 150 \times 150$ mm) with a 900 mm long bar embedded partially in the concrete cube. The embedment length was also designed in multiples of the bar diameter or side of the bar (see Table 9), being the diameter or side of the rods was 8 mm.

The two ends of the bar in the concrete cube were isolated from the concrete environment with plastic bushes (bond breakers). In previous trials and under high loads, it was seen that failure occurred in GFRP rods localised to areas near the devices for gripping the bar. Therefore, in order to avoid this premature failure, it was decided to reinforce the end of the square profile of GFRP with steel bushes. Both static (for the characterisation of the ultimate pull-out load) and dynamic tests were performed in the same machine. The load was applied by a hydraulic actuator equipped with an MTS load cell of 25 kN maximum capacity and an LVDT. The test was controlled using an MTS controlling unit and a data logger. The test set-up is presented in Fig. 8.

Static tests were primarily conducted to find an ultimate pull-out load as reference to establish load levels for running the dynamic tests. In this context, it must be highlighted that the great scatter of the static values could influence the development of the fatigue test. As before mentioned, factors such as process of manufacturing and set-up of the specimen may be responsible of such dispersion. Further number of specimens should have been tested to more exactly perform the fatigue study.

The dynamic tests were load controlled according to the load signal performing a sinusoidal movement. After the test specimens had been placed in the hydraulic jaws, the mean level of the function generator was increased from 0 to $(P_{max} + P_{min})/2$ and the load amplitude and frequency were preset before the test started. A counter automatically counted the cycles and stopped when the function generator did. In order to stop the test a maximum value for the ram displacement was preset. When this limit was exceeded, the function generator stopped automatically, so that the test did not have to be kept under observation constantly.

Tests were carried out at different load levels to construct stress versus number of cycles diagrams. The

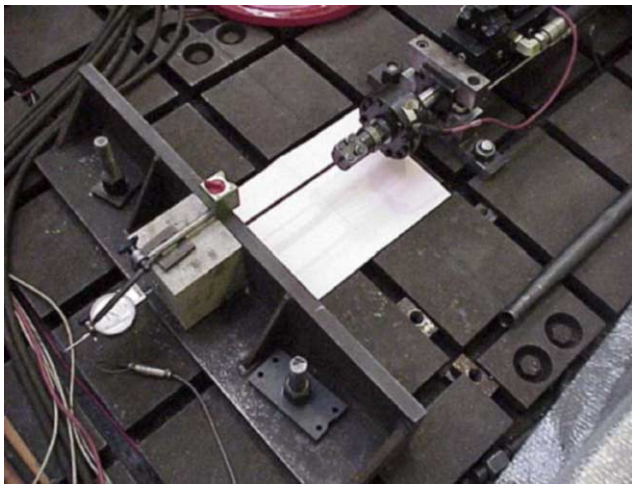

Fig. 8. Dynamic bonding test set-up.

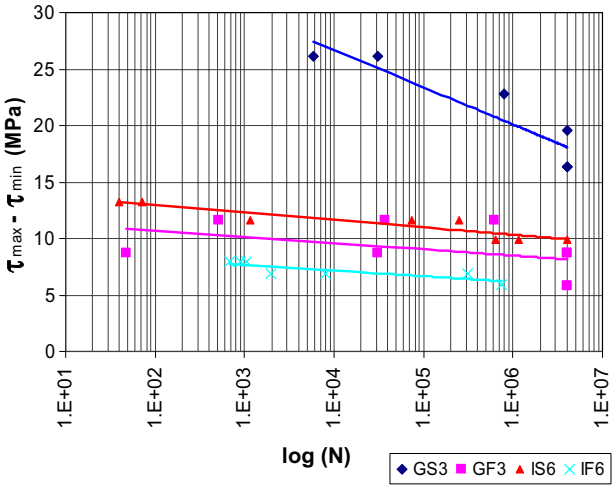

Fig. 9. ($\tau_{max} - \tau_{min}$)–log(N) relation in bonding under cycling loads.

cyclic load is applied until the specimen fails or the number of cycles reaches 4,000,000. At this number of cycles the tests are stopped. P_{max} was established as a percentage of the ultimate static pull-out strength. P_{min} was equal to $0.1 \cdot P_{max}$. The load frequency is 10 Hz ($T = 0.1$ s).

A total of 48 tests were performed to characterise the bonding fatigue behaviour on polymer concrete and cement concrete reinforced with FRP and steel. The 48 tests are divided into 4 Test Series named as GS3 (PPC type G with steel bars and 24 mm bond length), GF3 (PPC type G with GFRP bars and 24 mm bond length), IS6 (CC with steel bars and 48 mm bond length), and IF6 (CC with GFRP bars and 48 mm bond length).

Within every series, before performing fatigue tests, ultimate static pull-out loads on 3 specimens were obtained in order to define P_{max}, and consequently P_{min}. Once the static values had been obtained, the average of the 3 obtained results was calculated. This static average was considered constant for each series of test. In the bonding fatigue test, the failure is considered when the displacement exceeds that displacement corresponding to the mean value of the ultimate pull-out load. All the test results are illustrated in a diagram with the bonding stress range ($\tau_{max} - \tau_{min}$) along the axis of ordinate, and number of cycles along the logarithmic axis of abscises.

Fig. 9 shows all test results obtained in the dynamic test under cyclic loads in order to facilitate the comparison among the four types of specimens.

6.2.1. Results from the GS3 series

These PPC type G concrete blocks with steel bars static pull-out results are given in Table 14 and dynamic in Table 15. The maximum and minimum stress range for the dynamic test of this series are established according to above P_{max} and P_{min}, respectively.

Table 14
Static pull-out results for GS3 series tests

Specimen[a]	P_{ub} (KN)[b]	Displacement (mm)[c]	Failure type
GS3-01	24.32	2.26	Bond
GS3-02	22.36	2.28	Bond
GS3-03	18.93	2.38	Bond
Mean value	21.87	2.31	

[a] GS3 series are the pull-out specimens (orthophthalic PPC blocks) with embedded steel bars.
[b] P_{ub} = Ultimate static pull-out load.
[c] Measured in the free unloaded edge of the bar as included in Fig. 7.

Table 15
Bonding fatigue results for GS3 series tests

Specimen	Load level[a] (%)	Cycles N	Failure type[b]
GS3-04	80	5860	Bonding fatigue
GS3-05	80	30,688	Bonding fatigue
GS3-06	70	800,000	Bonding fatigue
GS3-07	60	4,000,000	1.56 mm slip
GS3-08	50	4,000,000	1.38 mm slip
GS3-09	50	4,000,000	0.90 mm slip

[a] Calculated from Table 14 P_{ub} value used for determining P_{max} and P_{min}.
[b] The failure under tensile occurred in bars are not considered in characterising the bonding fatigue.

For the test specimens of type GS3, it is evident that, for P_{max} equal to 50% of the Ultimate Static Strength, it is impossible to provoke a fatigue failure in the bond zone. However, during the test performance with the 50% load level, fatigue failure under tensile strength occurred in the reinforcement bars between the block and the gripping device. This failure might have been due to surface cracks along the reinforcement, and it was not

considered as failure when characterising the bonding fatigue.

6.2.2. Results from the GF3 series

These series *correspond* to the specimens of orthophthallic polyester polymer concrete blocks with GFRP bars. The static pull-out results are given in Table 16. The bonding fatigue results are given in Table 17.

Unlike the GS3 series, the FRP reinforcement bars did not show fatigue failure during testing procedure on GF3 series. For P_{max} equal to 60% of the Ultimate Static Strength, two specimens gave bonding fatigue failure before having reached 4,000,000 cycles and other two ones without bonding fatigue failure. For P_{max} equal to 40% of the Ultimate Static Strength, however, it is evident that specimens are below their bond fatigue limit. Therefore, fatigue limit can be said to be close to 60% of the Ultimate Static Strength, but more tests would be necessary to obtain accurate results.

6.2.3. Results from the IS6 series

These series correspond to the specimens of ordinary cement concrete blocks with steel bars. The static pull-out results are given in Table 18. The bonding fatigue results are given in Table 19. Like the GS3 series, the steel bars present fatigue failure, and it avoids characterising accurately the bonding fatigue. Different results were observed at 60 % of the Ultimate Static Strength, and consequently it is not either possible to give any definitive prediction concerning the fatigue limit. Nevertheless, according to the tendency line, the fatigue limit may be also lower than 60%. Finally, it can be also remarkable that bond failure occurs at very few cycles for load levels of 80%.

Table 16
Static pull-out results for GF3 series tests

Specimen[a]	P_{ub} (KN)[b]	Displacement (mm)[c]	Failure type
GF3-01	11.95	1.70	Bond
GF3-02	14.01	1.31	Bond
GF3-03	11.03	3.08	Bond
Mean value	12.33	2.03	

[a] GF3 series are the pull-out specimens (orthophthalic PPC blocks) with embedded FFRP bars.
[b] P_{ub} = Ultimate static pull-out load.
[c] Measured in the free unloaded edge of the bar as presented in Fig. 7.

Table 17
Bonding fatigue results for GF3 series tests

Specimen	Load level[a] (%)	Cycles N	Failure type[b]
GF3-04	80	623,530	Bonding fatigue
GF3-05	80	37,650	Bonding fatigue
GF3-06	80	516	Bonding fatigue
GF3-07	60	30,700	Bonding fatigue
GF3-08	60	47	Bonding fatigue
GF3-09	60	4,000,000	1.76 mm slip
GF3-10	60	4,000,000	0.80 mm slip
GF3-11	40	4,000,000	0.35 mm slip
GF3-12	40	4,000,000	0.07 mm slip

[a] Calculated from Table 16 P_{ub} value used for determining P_{max} and P_{min}.
[b] Fatigue limit can be said to be closed to 60% of the ultimate static strength.

Table 18
Static pull-out results for IS6 series tests

Specimen[a]	P_{ub} (KN)[b]	Displacement (mm)[c]	Failure type
IS6-01	20.72	2.54	Bond
IS6-02	23.27	1.07	Bond
IS6-03	22.50	3.23	Bond
Mean value	22.16	2.28	

[a] IS6 series are the pull-out specimens (ordinary concrete CC blocks) with embedded steel bars.
[b] P_{ub} = Ultimate static pull-out load.
[c] Measured in the free unloaded edge of the bar as presented in Fig. 7.

Table 19
Bonding fatigue results for IS6 series tests

Specimen	Load level[a] (%)	Cycles N	Failure type[b]
IS6-04	80	71	Bonding fatigue
IS6-05	80	40	Bonding fatigue
IS6-06	70	25,3428	Fatigue of bar
IS6-07	70	1155	Bonding fatigue
IS6-08	70	73,640	Bonding fatigue
IS6-09	60	648,731	Fatigue of bar
IS6-10	60	4,000,000	0.33 mm slip
IS6-11	60	1,165,532	Bonding fatigue

[a] Calculated from Table 18 P_{ub} value used for determining P_{max} and P_{min}.
[b] Fatigue limit can be also said that occurs closed to 60% of the ultimate static strength.

6.2.4. Results from the IF6 series

These series correspond to the specimens of ordinary cement concrete blocks with GFRP bars. The static pull-out results are given in Table 20. The bonding

Table 20
Static pull-out results for IF6 series tests

Specimen[a]	P_{ub} (KN)[b]	Displacement (mm)[c]	Failure type
IF6-01	16.19	1.59	Bond
IF6-02	12.10	1.26	Bond
IF6-03	22.35	1.21	Bond
Mean value	16.88	1.35	

[a] IF6 series are the pull-out specimens (ordinary concrete CC blocks) with embedded GFRP bars.
[b] P_{ub} = Ultimate static pull-out load.
[c] Measured in the free unloaded edge of the bar as presented in Fig. 7.

Table 21
Bonding fatigue results for IF6 series tests

Specimen	Load level[a] (%)	Cycles N	Failure type[b]
IF6-04	80	1050	Bonding fatigue
IF6-05	80	681	Bonding fatigue
IF6-06	80	891	Bonding fatigue
IF6-07	70	312,810	Bonding fatigue
IF6-08	70	1951	Bonding fatigue
IF6-09	70	8022	Bonding fatigue
IF6-10	60	753,240	Bonding fatigue
IF6-11	60	177	Bonding fatigue
IF6-12	60	45	Bonding fatigue

[a] Calculated from Table 20 P_{ub} value used for determining P_{max} and P_{min}.
[b] Fatigue limit can be also said that occurs below 60% of the ultimate static strength.

fatigue results are given in Table 21. In these series the fatigue limit can be said to be below 60%.

From the results of the bonding fatigue tests, the following conclusions can be drawn:

- Due to extremely great scatter of results, it is difficult to give concluding remarks on the test results. More tests for every load level are necessary to obtain results for design purpose. The performed test series, therefore, give a qualitative indication of the bonding fatigue behaviour.
- The specimens are very sensitive to the testing procedure, and consequently unforeseen failures have occurred during the tests. On the one hand, some steel reinforcement bars failed before bonding fatigue occurred, and as consequence of the latter, it just can be said that bonding fatigue might happen with a number of cycles higher than those corresponding to the bar fatigue failure. Moreover, for some specimens subjected to 60% of Ultimate Static Strength, it was observed that some failed at low number of cycles, and others, however, reached their fatigue limit. Therefore, it can be concluded that factors such as casting, transportation, materials are determining and may cause great scatter of results as well as premature failures.
- From the results obtained in the tested series, the fatigue limit can be estimated around 50% of the Ultimate Static Strength, being the minimum stress equal to 0.1 maximum stress. For more accurate estimation, further specimens should then be tested.
- In previous tests carried out by Amnon [10], it was not found a relevant temperature rise resulting from friction between the concrete and the FRP rod. Therefore, the bonding fatigue failure is not expected to occur due to resin degradation of the FRP bar.
- Since some of the load levels are close to the yield strength of the steel bar, premature failures appear before bonding fatigue. The FRP rods, however, do not show fatigue under the test load levels. In order to avoid failures due to steel fatigue, the bonding length should be reduced in those specimens reinforced with steel bars.

Acknowledgements

The work presented in this paper was financed by European Commission under the Contract number BRPR-CT98-0708 (1998–2002) and the Spanish Government, as a national project, under the Contract number MAT98-1734-CE (1999–2001).

References

[1] San-José JT. Highly durable precasted special concrete reinforced with non-metallic rebars—Plasticrete, European Project contract BRPR-CT98-0708, Bilbao, Fundación Labein, 2002.
[2] Fowler DW. Polymers in Concrete—where have we been and where are we going? In: Proceeding International Congress on Polymers in Concrete, Hawai, 2001.
[3] Fowler DW. Structural design of polymer concretes. In: Third Southern African Conference on Polymers in Concrete, Johannesburg, 1997.
[4] Ramírez JL, San-José JL. Predictability of structural calculation values in a 100 MPa polymeric concrete. In: Proceeding International Congress on Polymers in Concrete, Hawai, 2001.
[5] RILEM. Symposium on properties and tests methods for concrete-polymer composites. Oostende; 1995; method TC 113-CPT (PC-8).
[6] San-José, JT. Structural and ornamental polymer concrete. Application to building composites. PhD thesis, Bilbao Basque Country University, 1996.
[7] San-José JT, et al. Fundamental aspects of polyester polymer concrete in relation with its internal structure and bonding response. Scientific Israel—Technologies advantages, No. 3–4, Civil Mater Eng 2003;4:32–48.
[8] ACI Committee 440. Guide for design and construction of reinforced concrete with FRP bars. ACI 440.1R-01 2001.
[9] Permanent Commission of Concrete CPH—Spanish Instruction EHE. Spain, 1999, in Spanish.
[10] Katz A. Bond to concrete FRP bars after cycling loading. J Composites Constr 2000;137.